Irish-type deposits in Tunisia: a new perspective to assign the Pb-Zn deposits of the Nefza District

Sophie Decrée[1], Alicia Van Ham-Meert[2], Jean-Marc Baele[3], Olivier Namur[2], Etienne Deloule[4] & Christian Marignac[5]

[1] *Royal Belgian Institute of Natural Sciences – Geological Survey of Belgium, B-1000, Brussels, Belgium.*

[2] *Department of Earth and Environmental Sciences, Katholieke Universiteit Leuven, B-3001 Leuven, Belgium*

[3] *Department of Geology and Applied Geology, University of Mons, B-7000 Mons, Belgium*

[4] *Université de Lorraine, CNRS, CRPG, F-54000 Nancy, France*

[5] *Université de Lorraine, CNRS, Géoressources, F-54000 Nancy, France*

Corresponding Author: James Conliffe JamesConliffe@gov.nl.ca

Irish-type deposits in Tunisia: a new perspective to assign the Pb-Zn deposits of the Nefza District

Sophie Decrée[1], Alicia Van Ham-Meert[2], Jean-Marc Baele[3], Olivier Namur[2], Etienne Deloule[4] & Christian Marignac[5]

[1] *Royal Belgian Institute of Natural Sciences – Geological Survey of Belgium, B-1000, Brussels, Belgium.*

[2] *Department of Earth and Environmental Sciences, Katholieke Universiteit Leuven, B-3001 Leuven, Belgium*

[3] *Department of Geology and Applied Geology, University of Mons, B-7000 Mons, Belgium*

[4] *Université de Lorraine, CNRS, CRPG, F-54000 Nancy, France*

[5] *Université de Lorraine, CNRS, Géoressources, F-54000 Nancy, France*

Abstract: In the Nefza district (Tellian Nappe Zone of northern Tunisia), the small post-nappe basins of Sidi Driss and Douahria host Messinian Pb-Zn sulphide ore. The latter occurs as early diagenetic replacement of host carbonates and sulphates. Textural evidence and sulphur isotope composition suggest that Messinian seawater and sulphates are the sulphur sources for sulphides. Both bacterially-mediated and thermally-driven abiotic chemical sulphate reduction processes are involved. Alternating sulphate reduction processes are due to the mixing of shallow-basinal and deeper - hot (T<150°C) - fluids. In the context of the Messinian extensional setting, these deposits are likely related to thermally driven fluid circulation linked to mafic magmatism. The regional structural discontinuities act as the main fluid conduits.

Based on their characteristics, the Sidi Driss and Douahria deposits can be regarded as hybrid deposits between Sedimentary-exhalative and Mississippi Valley-Type deposits, as are the Irish-type deposits. The Nefza deposits actually show many similarities with the latter, as both are characterised by: (i) the early (syndiagenetic) formation of the deposits, (ii) the spherulitic and colloform texture of sphalerite, with comparable Fe and Cd contents and δ^{34}S values (suggesting formation by biomineralization and testify to a dominant bacterially-mediated sulphate reduction process), (iii) the involvement of hydrothermal (medium to hot) fluids leading to thermally-driven abiotic chemical sulphate reduction process. Locally, these fluids are driven by heat induced extension-related magmatism (shallow convection cells), and finally (iv) the control of the Pb-Zn deposits by major deep inherited structures that underwent transtensional reactivation.

Keywords: Tunisia, Nefza District, Sidi Driss, Douahria, Messinian Stage.

Introduction

The Pb-Zn deposits of Tunisia constitute a mining province which has operated since the first part of the 20th century. Most of them are peridiapiric and interpreted as Mississippi Valley-Type (MVT) deposits resulting from a gravity-driven fluid circulation event related to late Alpine convergence and thrust sheet formation in the Maghrebide belt (Kyle & Posey, 1991; Perthuisot & Rouvier, 1996). By contrast, in the Nefza region (Tellian Nappe Zone, northern Tunisia, Fig. 1), the small Messinian Pb-Zn deposits (Sidi Driss and Douahria) clearly differ from the neighbouring MVT deposits. They are hosted within post-nappe continental basins and occur as early diagenetic replacement of carbonates and sulphates. In addition, they formed in an extensional setting and present a spatial and temporal link with Neogene magmatism. These deposits were classified as Sediment-Hosted Massive Sulphide (SHMS) – Sedimentary-exhalative (SedEx) deposits (Decrée *et al.,* 2008a,

2014, 2016), although they are missing key features of the SHMS-SedEx deposits *sensu stricto*, such as the formation by exhalative processes of these deposits and their common large size.

The aim of this contribution is to provide an up-to-date insight into the Nefza Pb-Zn deposits and further investigate the comparison of the Sidi Driss and Douahria deposits with the Irish-type deposits. In comparison to the Nefza Pb-Zn deposits, the Zn-Pb deposits hosted in carbonates of the Irish ore field are predominantly due to SedEx-type mineralizing processes (Wilkinson, 2014, and references therein). However, the Irish-type deposits, which share similarities with both MVT and SedEx deposits, are typically regarded as a hybrid class (e.g., Piercey, 2013; Yesares *et al.*, 2019). This contribution is based on data from the literature and new petrographic and geochemical observations, including Laser-Induced Breakdown Spectroscopy (LIBS) mapping of the textures of sulphides (Baele *et al.*,
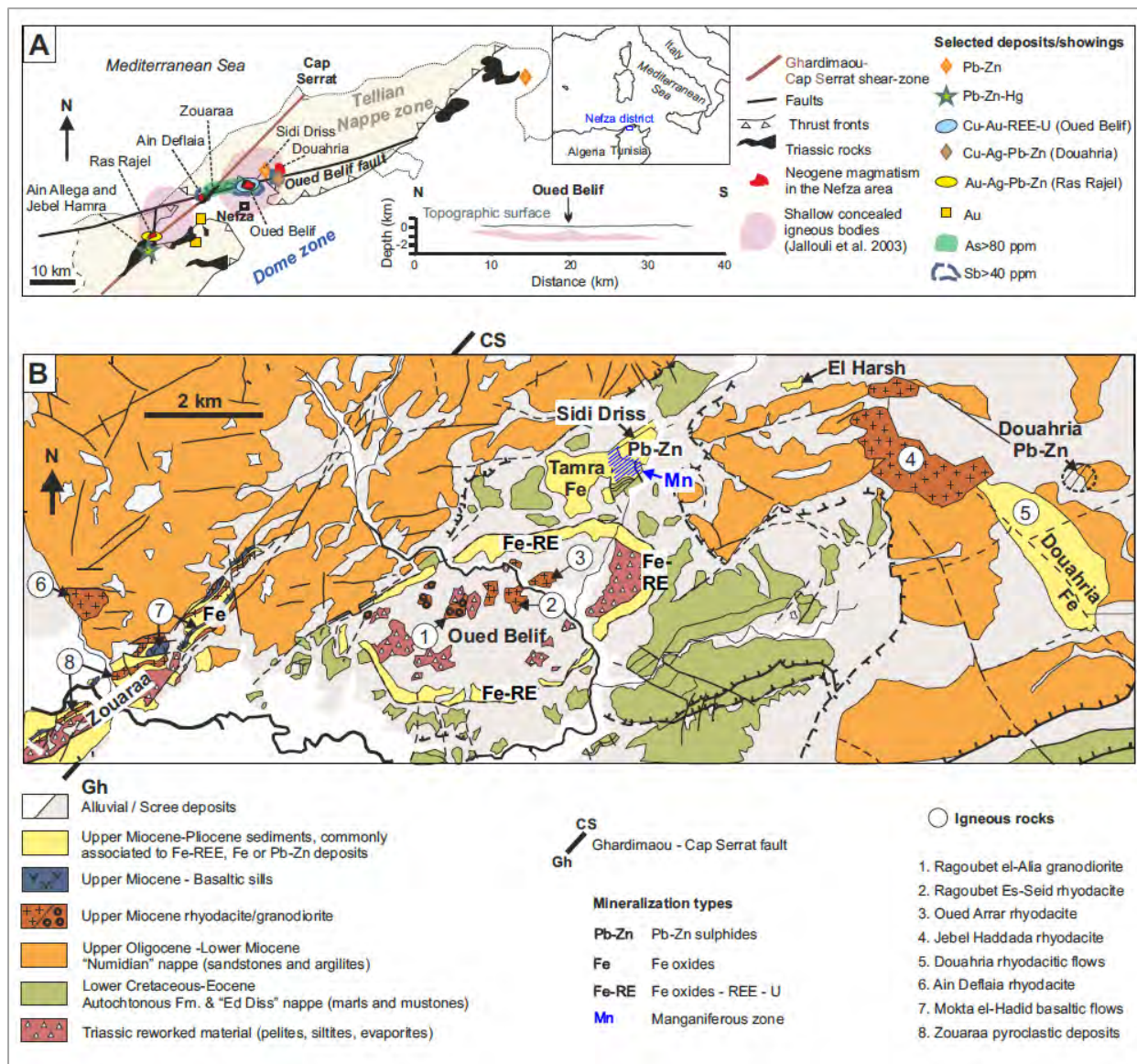
Figure 1: *A. Metal deposits, occurrences, and geochemical anomalies in relation with the structural setting of the Nappe Zone (Nefza District; modified from Gharbi, 1977; Albidon Limited, 2004; Decrée et al., 2013, 2014, 2016). The cross section illustrates the shallow concealed igneous body beneath the Oued Belif structure (modified from Jallouli et al., 2003); B. Geological sketch map of the Nefza district (modified from Gottis & Sainfeld, 1952; Batik, 1980; Rouvier, 1987, 1994; Decrée et al., 2014, 2016), showing the locations of selected deposits/occurrences and igneous rocks.*

2021) and Laser Ablation Inductively Coupled Plasma Mass Spectrometry (LA-ICPMS) analyses of sulphides.

Geological context

The Nefza district in the Tellian Nappe Zone

The Nefza district (Fig. 1) is located in the Tellian Nappe Zone, which is part of the Maghrebide belt. The latter resulted from the collision between the African plate and a microplate derived from the European continent during the Early Jurassic (Jolivet, 2008, and references therein). In northern Tunisia, the evolution of the fold-and-thrust belt started in the latest Burdigalian in the Internal Zone (that constitutes the northern part of

the Maghrebide belt) and ended in the Late Tortonian at the Tellian front (e.g., Bouaziz *et al.*, 2002; Benaouali-Mebarek *et al.*, 2006).

The sedimentary substrate of the Tellian Nappe Zone comprises the Adissa and Ed Diss thrust sheet (Upper Cretaceous to Eocene limestone and marl; Rouvier, 1977; Ould Bagga *et al.*, 2006) that is overlain by the Numidian nappe, which is a thick (up to 1500m) series of Oligocene to Lower Miocene siliciclastic flysch (Rouvier, 1977) (Fig. 1). The Numidian Nappe is thought to have been a flysch accretion prism emplaced first in the Internal Zone during the latest Burdigalian. It was then remobilized and integrated into the Tellian Zone as a nappe during the Tortonian before the folding of the whole nappe pile during the Late Tortonian (Khomsi *et al.*, 2009).

Extensional tectonics prevailed during the Late Tortonian-Early Messinian, and in the Pliocene (Bouaziz *et al.*, 2002; Belguith *et al.,* 2011; Booth-Rea *et al.*, 2018), and induced the formation of small continental basins in areas hosting Pb-Zn-Fe ore deposits. In the Nappe Zone, the NE-SW sinistral Ghardimaou-Cap Serrat fault zone (GCSFZ) (Rouvier, 1977; Mauduit, 1978) and a series of N80°E lineaments represent reactivated Hercynian structures (Melki *et al.*, 2012). These structures control most of the post-collisional magmatism and location of most ore deposits and showings. Zn-Pb-Ba-Sr deposits and As anomalies occur along both trends (Fig. 1A), whereas REE, Au and Sn-Sb occurrences/anomalies are restricted to N80°E lineaments.

In the Tellian Nappe Zone, late Serravallian-Messinian felsic and mafic magmatism postdate the thrusting (Jallouli *et al.*, 2003 and references therein). Many of these magmatic rocks are encountered in the Nefza district (Fig. 1B):

(i) the Serravalian Ragoubet el-Alia granodiorite (12.9 ± 0.5 Ma; Bellon, 1976; Faul & Foland, 1980) and the Tortonian Ragoubet Es-Seid and Oued Arrar rhyodacites (8.3 ± 0.8 and 8.9 ± 0.15 Ma; Badgasarian *et al.,* 1972; Faul & Foland, 1980) that are likely rooted in a very shallow concealed magmatic sill (0.5-1.5km in depth, 0.7-0.9km in thickness, diameter of ca. 20km), which was recognized over the whole study area by geophysical surveys (Fig. 1A; Jallouli *et al*., 2003).

(ii) The Jebel Haddada massif comprises a rhyodacitic dome (8.7 ± 0.15 Ma - 8.2 ± 0.4 Ma; Bellon, 1976; Faul & Foland, 1980) and volcanic ash within the Douahria Fe-rich sedimentary rocks.

(iii) The Ain Deflaia dome, comprised of cordierite-bearing rhyodacite (dated at 8.5 Ma; Rouvier, 1977), with related pyroclastic deposits in the neighbouring Zouaraa basin (Laridhi-Ouazaa, 1996).

(iv) Transitional basalt sills (Zouaraa basin, dated at 6.9 ± 0.3 Ma and 6.4 ± 0.15 Ma by Rouvier, 1977), related to Messinian extensional conditions (e.g., Mauduit, 1978; Maury *et al*., 2000; Jallouli *et al*., 2003; Decrée *et al.,* 2014).

The granodiorite and rhyodacite are likely sourced from a metaluminous calc-alkaline magma mixed with variable proportions of melted continental crust (Maury *et al*., 2000; Decrée *et al*., 2014). The transitional basalts derived from an enriched mantle source at the lithosphere-asthenosphere boundary (Maury *et al*., 2002; Decrée *et al*., 2014). They emplaced along lithospheric-scale shear-zones inherited from the Variscan orogeny (Piqué *et al*., 1998, 2002). Magma ascent in the Tellian Zone was likely facilitated by the thinner lower crust (10km in the Tellian Zone vs. 20km in Central Tunisia; Jallouli & Mickus, 2000) and a more proximal Moho (~25km; Mickus & Jallouli, 1999).

Mineral deposits in the Nefza district

In the Nefza district, the Oued Belif mineralized breccia is a distinct feature forming an elliptical ring ~7 x 3 km in size that encloses two generations of shallow felsic magmatism and Triassic diapiric materials. Fine-grained hematite constitutes most of the breccia matrix. It is associated with REE (LREE), U minerals and Au showings (Albidon Limited, 2004), possibly of IOCG-type (Decrée *et al.*, 2013). The Oued Belif geochemical features suggest a contribution from felsic and mafic magmatism (Decrée *et al*., 2013).

Other key deposits in the area are the Messinian Pb-Zn deposits that are hosted in the small, post-nappe, continental to shallow open-marine extensional basins of Sidi Driss and Douahria. The Sidi Driss ore was exploited for Pb and Zn ore for more than a century and the mine closed 30 years ago. It is now exhausted. Since this paper focuses on these deposits, their detailed description is provided below.

A second generation of small Mio-Pliocene basins hosts Fe ore in the area. The Pliocene Tamra basin, that partly overlies the Sidi Driss basin, hosts a 50m-thick succession of iron hydroxide-bearing sediment sequences, which resulted from combined sedimentation of iron-rich lateritic material and in situ pedogenetic reworking (Decrée *et al.*, 2008b; Yans *et al*., 2021). Its eastern part, known as the "manganiferous zone" (Fig. 1B), is highly mineralized in Mn, Pb, Zn, Ba and Sr, due to hydrothermal fluid circulation that leached the underlying Sidi Driss ore during the Pliocene (Decrée *et al*., 2010; Garnit *et al*., 2020; Dekoninck *et al*., 2018). The Douahria basin is another post-nappe basin, the infilling of which (conglomeratic/argillitic formations with volcanoclastic intercalations) is heavily Fe impregnated (Negra, 1987).

Overview of previous work and new data

Volcano-sedimentary context of the mineralized Sidi Driss and Douahria basins

The Sidi Driss and Douahria basins unconformably overlie the eroded nappe pile forming the regional substratum. The sediments filling these basins are mainly Messinian in age based on their evaporitic depositional environment, the presence of lignite and cross stratification at Sidi Driss (Sainfeld, 1952) as well as mammalian fossils from the Pikermi fauna of latest Messinian age (Roman & Solignac, 1934; Jaeger, 1977). However, a contribution from late Tortonian sediments is likely considering the occurrence of volcanoclastic strata related to Tortonian felsic magmatic activity. In both basins, the depositional environment of the sediments was shallow, with shallow marine sediments and input from the landmass and fluviatile sedimentation as the latest infilling of the basins. The Zn-Pb sulphide mineralization is hosted in shallow marine limestones that consist of interbedded micritic and anhydrite-bearing stromatolitic limestones in both basins.

Petrography and paragenetic sequence

Petrographical studies of mineralized samples from Sidi Driss and Douahria have been extensively carried out previously (e.g., Dermech, 1990; Decrée *et al.*, 2008a). This section is largely based on these works, presenting the most important features of the deposits.

At Sidi Driss and Douahria, the Pb-Zn ore is mostly stratabound (Fig. 2A,E) and composed of galena, sphalerite and Fe sulphides (pyrite and marcasite). It is banded or disseminated (Fig. 2A, C, E), replacing the host rock or filling voids. Rhythmic alternating mineralized layers is commonly observed (Fig. 2A, E). The syndiagenetic origin of these deposits is suggested
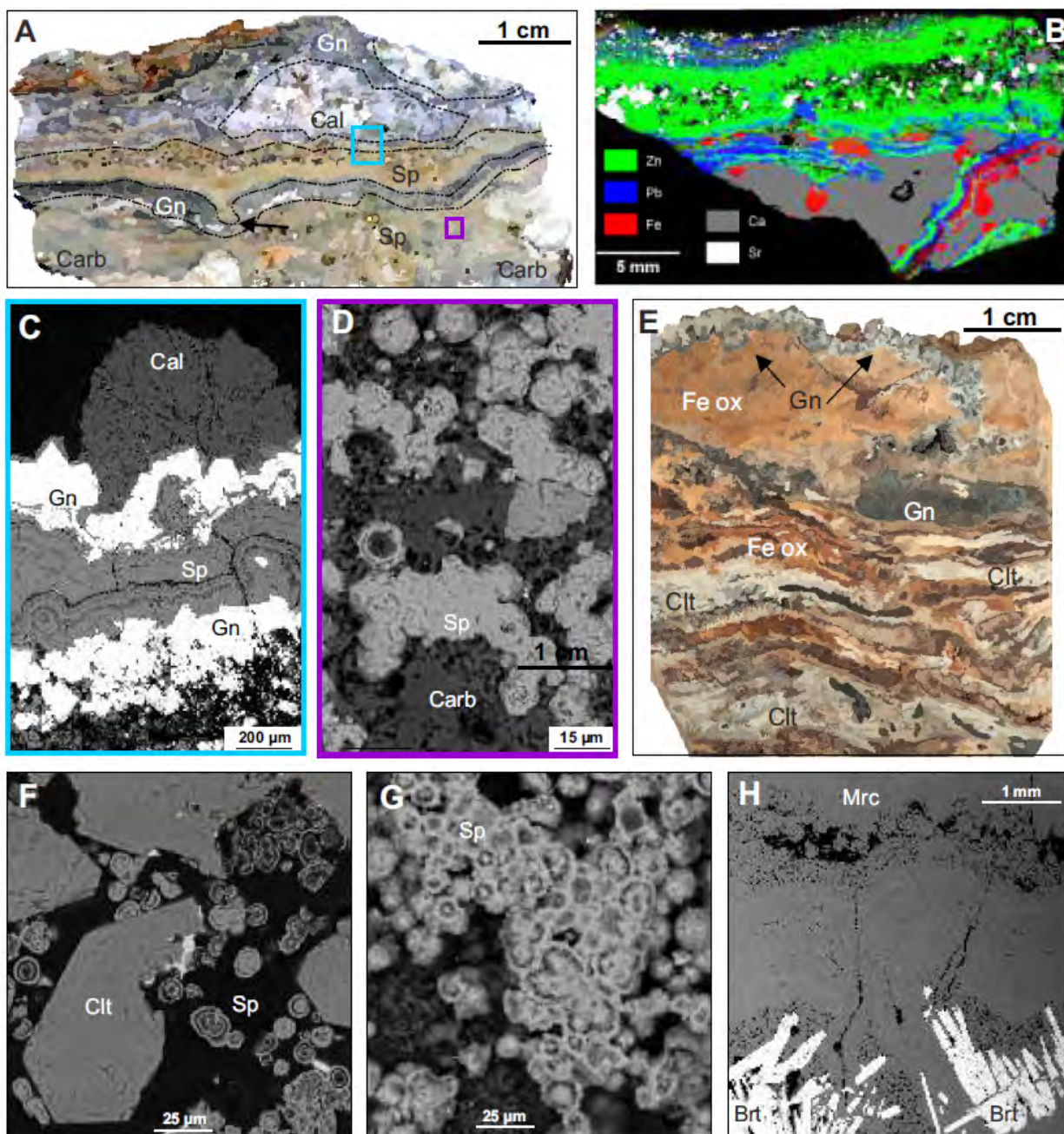
Figure 2*: Photographs (**A,E**), Scanning Electron Microscopy (SEM) backscattered electron images (**B,C, D, F-H**), and LIBS image of Pb-Zn ores from Sidi Driss (A-C,G) and Douahria (D-F) deposits; Brt-barite, Cal-calcite, Carb-carbonate, Clt-Celestite, Fe ox-iron oxides, Gn-galena, Mrc-marcasite, Sp-sphalerite (mineral names abbreviated according to Warr, 2021).*

A. *Alternating galena and sphalerite layers exhibiting early soft-sediment deformation (loadcast indicated by arrow) in carbonate host rock (sample SD2a(04); figure modified from Decrée et al., 2008a,2016).*

B. *General texture of the ore; Pb for galena, Zn for sphalerite, Fe for marcasite, Sr for celestite and Ca for calcite (methodology is provided as Supplementary material, Item 1).*

C*. Detail of the zone defined by the blue frame illustrated in (A): the colloform sphalerite layer is likely made up of coalesced spherules, whereas galena displays euhedral habit; remaining voids are filled with pyrite and calcite.*

D. *Detail of the zone defined by the violet frame illustrated in (A): coalescing sphalerite spherules in a carbonate host rock.*

E. *Stratabound ore made of alternating celestite, galena and Fe oxides layers (sample DSU1).*

F*. Detail of typical sphalerite spherules within celestite (sample DSU2).*

G. *Sphalerite spherule aggregate in a celestite host rock (sample DSU6).*

H. *Colloform band of marcasite after large barite euhedral laths (sample SD-Py5). More details are provided in the text.*
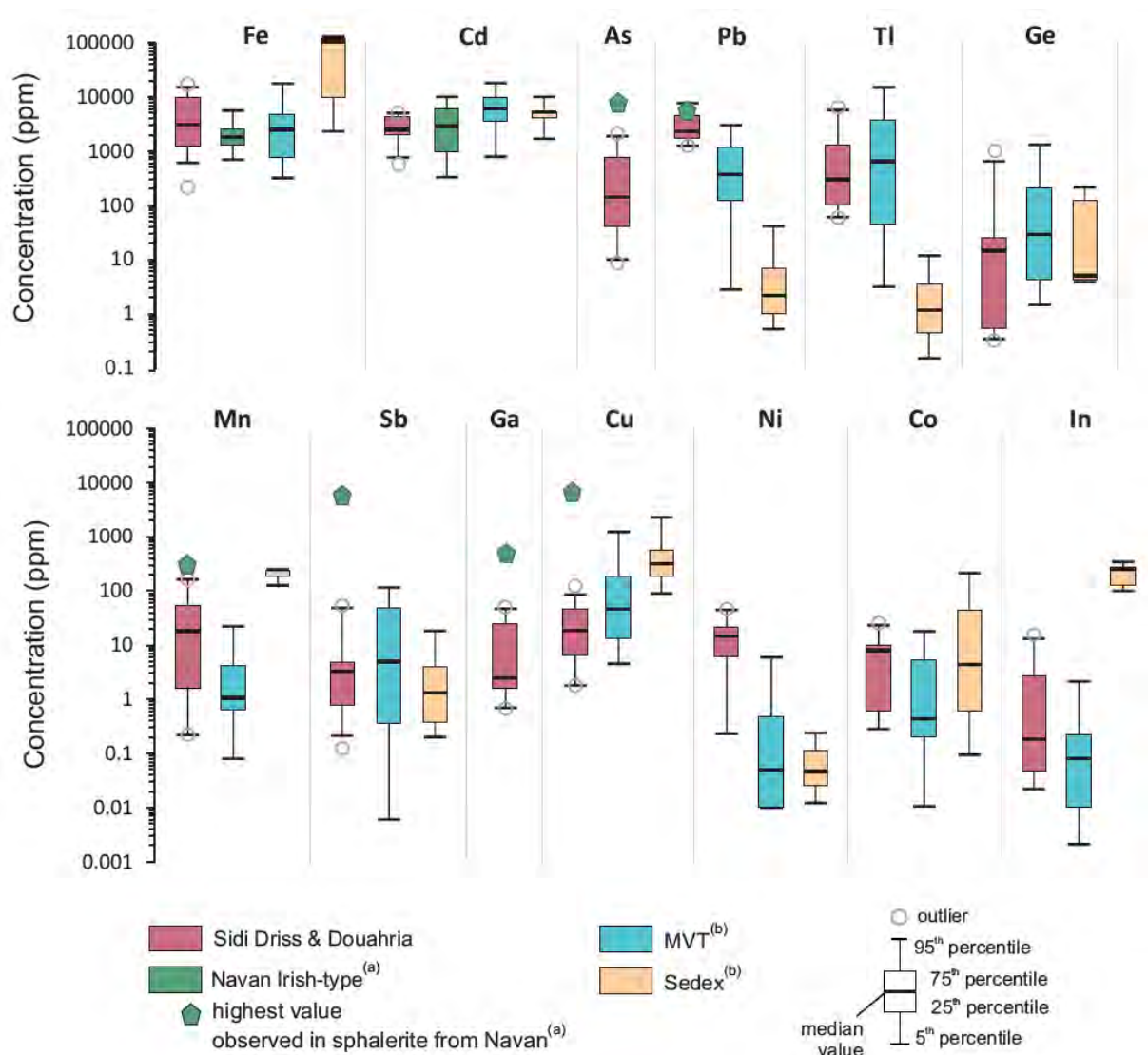
Figure 3: Box plots showing variation of several key major, minor and trace element contents (LA-ICPMS analyses) for 11 sphalerites from Sidi Driss and Douahria. Data for sphalerite from MVT and SedEx deposits (Hu et al., 2021, and references therein) and from the Navan Irish-type deposit are illustrated for comparison purposes. Note that only the highest value is represented for the Navan Irish-type deposits, the lowest value being under the detection limit (Gagnevin et al., 2014, and references therein). Data are summarized in the Supplementary material, Item 1 and the complete dataset is provided in the Supplementary material, Item 2.

by soft-sediment deformation, such as the loadcast structure in a galena layer shown in Figure 2A (Decrée *et al*., 2008a)

At Sidi Driss, the Zn-Pb-Fe sulphides are mostly hosted in early diagenetic Fe-Mn rich microsparite (a recrystallized algal boundstone, with up to 4.97 wt.% Fe and 1.84 wt.% Mn; Decrée *et al.,* 2008a) containing evaporite remnants (Fig. 2A-D). The primary host rocks were likely dolomite and Ca-sulphate-bearing sabkha sediments developed at the expense of algal mats. It was then modified by a dedolomitization process in the presence of Mn-Fe rich fluids (Decrée *et al*., 2008a). This process is common in shallow environments, where dolomite comes into contact with meteoric fluids (Sanz-Rubio et al., 2001). Carbonates were in turn partly replaced by sulphates - i.e., barite and celestite - that occur as massive stratabound equigranular aggregates (Decrée *et al*., 2008a). Barite can also

form later in the paragenetic sequence and recrystallizes as a network of large euhedral laths (up to a few mm, Fig. 2H) that are roughly coeval with sulphides. At Douahria, sulphides are mostly hosted by celestite (Fig. 2E, F), and then by highly recrystallized, dedolomitized limestones, with calcite containing up to 1.97 wt.% Fe and 0.81 wt.% Mn (Decrée *et al*., 2008a).

The base-metal mineralizing event led to the partial matrix dissolution/replacement of the carbonate/sulphate host-rock by sphalerite, galena and Fe-sulphides. These sulphides commonly form disseminated patches or layers. Massive replacement and coalescence of disseminated sulphides occur more frequently in the vicinity of some large voids/fissures. In both deposits, sphalerite exhibits spherulitic textures, with spherules being typically up to 30µm in diameter (Fig. 2D, F, G; as also observed by Abidi *et al*., 2022). Considering the

similarities with the "peloids" described by Kucha *et al.* (2010), they are interpreted as products of microbial activity. Both concentric zoning (Fig. 2D, F, G; with kaolinite or carbonate forming the darker layers; Decrée *et al.,* 2008a) and radial growth structures are observed within the spherules. In the zones where the ore is more massive, sphalerite typically occurs as colloform bands (Fig. 2A-C). Relict shapes of spherules in these suggest that –at least locally – colloform sphalerite results from the progressive recrystallization (through the early burial diagenesis) of a spherulitic horizon. By contrast, galena mostly forms euhedral to subhedral crystals/grains, with a size ranging from a few tens of microns to several millimeters (Fig. 2A, B, C, E). Galena frequently replaced sphalerite, as shown by corroded boundaries between massive sphalerite and galena (Decrée *et al.* 2008a). Pyrite and marcasite replaced earlier carbonates and/or sulphides and filled voids. Marcasite is usually present as colloform bands (from a few tens of µm to 1 cm in thickness, Fig. 2H) or displays radial textures (Fig. 2B, C). Calcite with a typical sparitic facies (with Mn contents of 3.35 wt.%; Decrée *et al.* 2008a) fills most of the remaining voids in the carbonate host rock Fig. 2A, C).

Late oxidation of the sulphide assemblage is particularly well expressed at Douahria, where late crystallization of iron oxides took place. One of the most distinctive features at Douahria is that celestite hosts the mineralization, where pure celestite layers alternate with galena layers (a few mm in thickness). Iron oxides, as hematite and goethite, partially fill the porosity (Fig. 2E). Galena is partly transformed into anglesite.

Sulphide chemistry

The chemistry of the sulphides at Sidi Driss and Douahria was only briefly addressed in the past, based on electron microprobe analyses (e.g., Dermech, 1990; Decrée *et al.*, 2008a). This section presents new data obtained by LA-ICPMS (methodology is provided as Supplementary material, Item 1). Statistics about the absolute concentrations for selected elements are provided in Figure 3 (the corresponding data are provided as Supplementary Material, Items 2 and 3).

In both deposits, Fe, Cd and Tl contents of sphalerite are variable, but low in iron (215<Fe<15304 ppm, with median value ("mv") of 3048 ppm Fe), and high in cadmium (595<Cd<15881 ppm, mv of 2704 ppm Cd) and thallium (69<Tl<8120 ppm, mv of 353 ppm Tl). Lead is also enriched in the sphalerite of these deposits, with concentrations varying from 1068 to 4962 ppm. Arsenic contents are high in sphalerite from Sidi Driss (127-1989 ppm), but lower at Douharia (7.5-117 ppm As). Germanium content is usually low in both deposits (0.3-30 ppm) but can reach 354 and 1009 ppm in sphalerite from Sidi Driss. Copper contents vary between 1.7 and 135 ppm, and Ni, Co, and In concentrations range from below detection limit to 46, 26 and 17 ppm, respectively. Mn, Ga and Sb concentrations are low and variable in both deposits (0.2-161 ppm Mn, 0.6-52 ppm Ga, 0.1-53 ppm Sb).

Arsenic and Tl are the main minor and trace elements in galena from Sidi Driss and Douahria, though with wide concentration ranges (from 1.7 to 4472 ppm, and from 15.5 to 2481 ppm respectively). Iron and Zn contents are low (7<Fe<60 ppm, 0.7<Zn<21 ppm), whereas Mn and Ge concentrations are very low (0.01-3.6 ppm for Mn, and 0.1-0.5 ppm for Ge). Antimony concentration in galena varies over two orders of magnitude, from below detection limit to 683 ppm. Cadmium, Cu, Ni and Co concentrations are low to very low (up to 49 ppm Cd, up to 1 ppm Cu, up to 0.3 ppm Ni, and up to 0.1 ppm Co). Ga and In contents are below detection limits.

Marcasite was only analysed in the Sidi Driss samples. It is characterized by usually high but rather variable As and Tl contents (1.7-4477 ppm for As, 0.1-0.5 ppm for Tl), whereas Zn, Ge, Sb are low (4.7-21 ppm Zn, 0.3-1.4 ppm Ge, 0.1-0.4 ppm Sb). The concentrations of other elements, such as Cu, Co, Ni, Ga, Cd and In are mostly below the detection limit. Wide ranges of concentrations are observed for Pb and Mn. They are related to the host rock in which the marcasite formed. Marcasite from the carbonate host rock (SD2a-Py1-3) has lower Mn and higher Pb contents (about 0.4 ppm Mn, 5023<Pb<6419 ppm), compared to marcasite crystallizing after barite formation (PY5-Py1-2) (123 and 299 ppm Mn, 2.7 and 3.8 ppm Pb).

Fluid inclusion studies

Measurements were performed on primary and other two-phase fluid inclusions found in late calcite which filled the remaining voids subsequent to sulphide deposition (sample SD 04/5). The primary inclusions range from 7 to 50µm in size, with a gas-to-liquid volume ratio between 0.05 and 0.20 and homogenize in the liquid state. The other fluid inclusions (forming small clusters of inclusions being of 4-30µm in size) also homogenize in the liquid state, with a gas-to-liquid volume ratio ranging from 0.05 to 0.15. In the selected sample, few fluid inclusions - whatever their type - permitted the measurement of ice melting temperature and bulk homogenization temperature. The first ice melting temperatures are between –21.4 and –21.7°C. This shows that NaCl is the dominant salt component. According to the NaCl-H₂O thermodynamic model system (Bodnar, 2003), the salinities corresponding to the ice melting temperature are of 18.3 to 11.7 wt % equivalent NaCl. A fluid mixing can explain this variation in salinities, by involving (i) a brine end-member (≥ca 20 wt % equivalent NaCl), which could be hypersaline Messinian seawater (≥350 g l-1: Flecker *et al.,* 2002) or result from interactions with the evaporitic rocks partly forming the Oued Belif Triassic diapir, and (ii) a low-salinity – meteoric – end-member. Since no Na to Ca exchange occurred during brine evolution (based on constant first ice melting temperatures), the fluid circulation occurred over a rather short distance. The bulk homogenization temperatures for the same inclusions are between 160° and 190°C.

A very shallow emplacement level for the mineralization is considered owing to the fact that there is no evidence of post-trapping modification, and the homogenization temperature values are likely to be close to the true trapping temperatures. No correlation exists between salinity and temperature variations. It is worth mentioning that the fluids observed here significantly differ from the fluids related to the genesis of the MVT deposits in the Tunisian Trough (e.g., Bougrine) , in connection with the Triassic diapirs. The latter indeed present
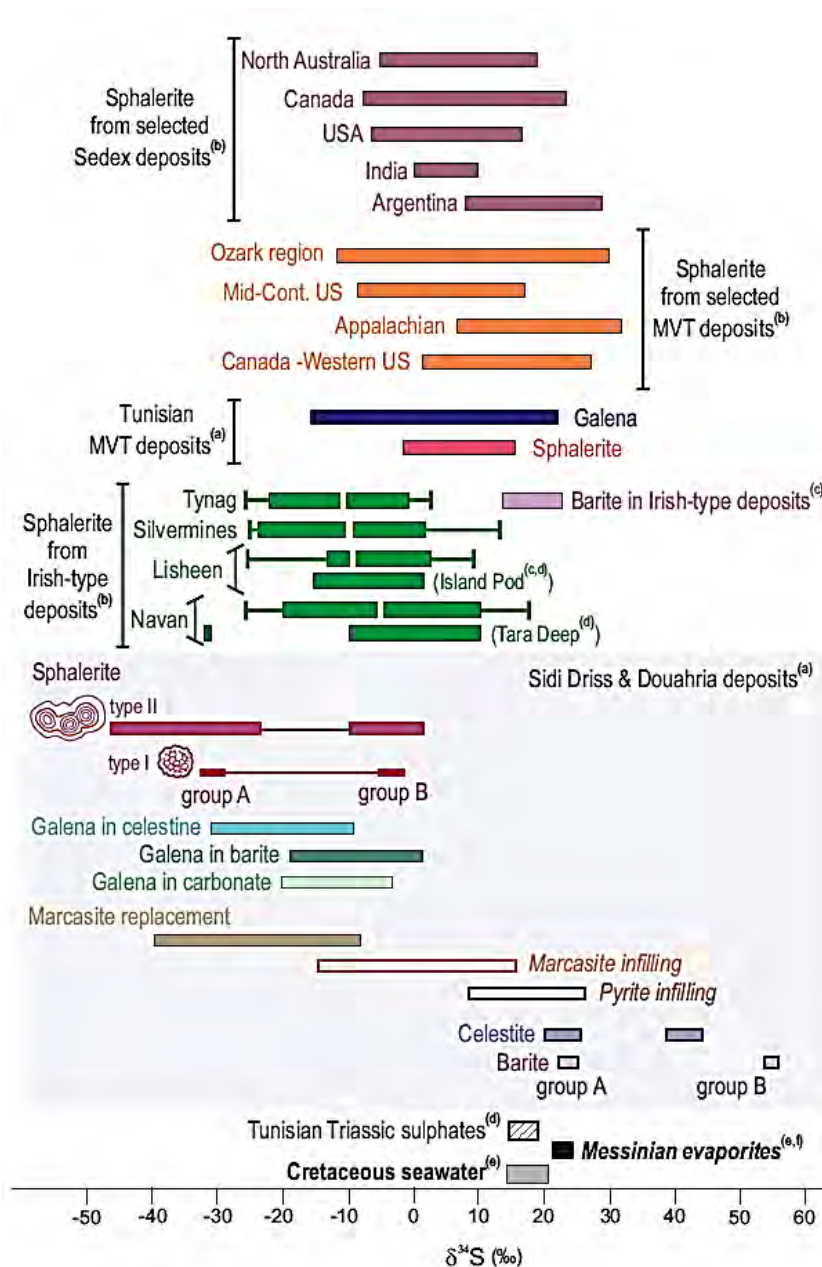
Figure 4: *Comparison of sulphur isotope values for ore deposits and occurrences in Tunisia and for sphalerite from deposits representative of the Irish-type, MVT and SedEx type. The total range of data is illustrated for MVT, SedEx and Sidi Driss and Douahria deposits. For the Irish-type deposits the total range of data is shown by the horizontal bar, the median value is indicated by the vertical white line, the 25th and 9th percentiles correspond to the extent of box. Data are from: (a) Decrée et al. 2016 (and references therein), (b) Leach et al. (2005), and references therein), (c) Yesares et al. (2019), (d) Sheppard et al. (1996), (e) Claypool et al. (1980), (f) Paytan et al. (1998).*

higher salinities (18-23 wt % equiv. NaCl) and lower homogenization temperatures, varying between 70 and 130°C (e.g., Charef & Sheppard, 1987; Sheppard *et al*.,1996).

Sulphur isotope composition

The following summary is mostly based on the work of Decrée *et al.* (2008a).

Both sulphates and sulphides were analyzed for their sulphur isotope composition. Two populations were identified for the sulphates (Fig. 4). The celestite and barite matrix (Group A in Fig. 4) exhibit $\delta^{34}S$ values varying from +21.5 to +24.4‰. The latter are in the range of Messinian evaporites (from +20.7 to +24‰; Claypool et al., 1980), suggesting that sulphates are derived from Messinian Ca-sulphates. In contrast, late barite euhedral laths (Group B in Fig. 4) are characterized by higher $\delta^{34}S$ values (from +40.7 to +57.0‰). Sphalerite spherule aggregates from Sidi Driss are characterized by a bimodal distribution of $\delta^{34}S$, with very light values (from −24.7 down to −43.9‰, Group A in Fig. 4) and heavier values (−8.1 to

+1.2‰, Group B in Fig. 4) (Filoche & Flinois, 2007 in Decrée *et al.,* 2008a). Galena display negative δ^{34}S values (−30.3 to −2.0‰), without any significant variation at the crystal scale or relationship with the host rock. Variability showed by Fe-sulphides is even larger, with both positive and negative values (δ^{34}S from −35.9 to +25.8‰). Intra crystal variability is also observed. Higher values were obtained on late pyrite infillings at Sidi Driss (δ^{34}S from +9.0 to +25.8‰), whereas marcasite from Douahria and Sidi Driss show lower values (from −35.9 to +16.8‰).

The obvious textural replacement of early sulphates by sulphides strongly supports that the former is a sulphur source for the latter, at least locally. In carbonate host rocks, early sulphides could have directly scavenged their sulphur from Messinian seawater or from the sulphates they replace. Alternative sulphur sources are the deeper Triassic sulphates that are present regionally, as stated below. Sulphur isotopic fractionation related to sulphate reduction depends on the reducing processes considered (e.g., Machel, 2001), with either a low-temperature bacterially-mediated reduction process (BSR) or a thermally-driven abiotic chemical reduction process (TSR). The microspherulitic texture of sphalerite strongly supports their biogenic nature (biomineralization) and BSR. In an open system, the latter results in ^{34}S fractionations of Δ^{34}S≫−20‰ (Machel, 2001). This is consistent with the most negative δ^{34}S values for sphalerite at Sidi Driss (from −24.7 down to −43.9‰, Group A), considering Messinian seawater or the early sulphates as the sulphur source. By contrast, the second group δ^{34}S values for sphalerite (Group B, δ^{34}S from −8.1 to +1.2‰) could be achieved through BSR in a closed system where sulphate supply is limited, through Rayleigh fractionation (Bechtel *et al.,* 1996).

The wide range of δ^{34}S values for galena (between −30 and −2‰), may be explained by somewhat different processes. First, galena at Sidi Driss and Douahria is mostly subhedral to euhedral and does not exhibit the typical textures of BSR-linked galena (e.g., Schroll, 1996). The very light sulphur isotope values (δ^{34}S down to −30‰) measured in some galenas could be inherited from the dissolution of pre-existing sphalerite that is replaced by galena, as frequently observed in the samples in both sites. Moreover, the inferred numerous dissolution events would account for an increase in the porosity and therefore permeability in the system. Considering the regional context (magmatism and high geothermal gradient, up to 100 °C·km^{-1}; Jallouli *et al.,* 1996), hydrothermal fluids could bring to the system a deep, heavy source of sulphur, that involves TSR (Machel, 2001). Because TSR fractionation results in ΔS≥−20‰ (Machel, 2001), the observed δ^{34}S values of sulphides can be obtained through TSR from diverse primary source, either Messinian sulphates (in-situ origin) or Triassic sulphates. As pointed out by Machel (2001) and Barre *et al.* (2017), the presence of reduced sulphur is a prerequisite to initiate the TSR reaction; at Sidi Driss, this prerequisite was fulfilled through the previous BSR.

The wide range of δ^{34}S values in marcasite (from -36 to +26 ‰) likely result from the replacement of early formed sulphides by Fe-sulphides. In late infillings, Fe sulphides can have high δ^{34}S values that would support Rayleigh fractionation in

a closed system, with early TSR-related sulphides enriched in ^{32}S and later sulphides enriched in ^{34}S. The same reasoning can be applied to the very wide range of δ^{34}S displayed by the late barite (Group B) that precipitated after light (^{32}S)-enriched Fe-sulphides.

Lead isotope composition

The lead isotope compositions were obtained on galena from the Sidi-Driss and Douahria deposits and compared to the signature of the sedimentary rocks forming the substrate and the igneous rocks – felsic and mafic – occurring in the vicinity of the Pb-Zn deposits (see Decrée, 2008 and Decrée *et al.,* 2014 for more details about the methodology). The Pb isotope compositions of galena from both deposits are variable - $15.670<^{207}$Pb$/^{204}$Pb<15.674; $18.772<^{206}$Pb$/^{204}$Pb<18.812; $38.848<^{208}$Pb$/^{204}$Pb<38.888 - and display a trend extending over the Nefza felsic magmatic rocks and their substratum, suggesting that the lead, and possibly other metals found in the ore do not originate solely from magmatic rocks but also from the rocks surrounding the ore deposits. The metals could have been leached from these formations by regional fluid circulation, with major structural discontinuities acting as main fluid conduits (Decrée *et al.,* 2008a).

Proposed model for the mineralization at Sidi Driss and Douahria

This section presents a summary of the main lines of reasoning and conclusions about the genetic model proposed for the Pb-Zn Sidi Driss and Douahria deposits by Decrée *et al.* (2008a, 2016). First of all, textural, geochemical and isotopic data studies highlight the complex and multi-stage nature of the mineralization and its early/syn-diagenetic (Messinian) character. This is particularly evidenced by the soft-sediment texture of the ore, the early Mn-Fe enrichment of the host carbonates, and the (sub-)contemporaneous sulphur source (Messinian seawater and/or early celestite/barite). The wide range of δ^{34}S values measured in sphalerite, galena and Fe-sulphides is interpreted as the result of alternating BSR fractionation (based on the observation of the microspherulitic sphalerite of likely biogenic origin) and TSR fractionation, which would be efficient at temperature above ~100°C (Machel, 2001). This temperature is consistent with the frequent replacement of sphalerite by galena, considering that the inversion in the relative solubility of these two sulphides occurs at around 150 °C (Barrett & Anderson, 1988; Seward & Barnes, 1997). Homogenization temperatures obtained on late calcite infillings (between 160 and 190 °C) also argue for the circulation of hot fluids. The thermally driven fluid circulation was likely linked to the Messinian mafic magmatism (Decrée *et al.,* 2008a) and/or to a concealed igneous sill at shallow depth (Jallouli *et al.,* 2003). Both would allow for the inception of small and shallow convection cells and provide the heat source for the high temperature (≥150 °C) fluids needed for TSR. The temperature fluctuations recorded by the alternating deposition of BSR and TSR-related sulphides suggest the mixing of shallow-basinal and deeper fluids. In that context, structural discontinuities, such as thrust sheet boundaries, magmatic contacts, and deformed diapirs, likely served as channels for efficient fluid flow (Decrée *et al.,* 2008a). Fluid circulation along these conduits would lead to

the metal leaching from both igneous and sedimentary substratum rocks, as suggested by lead isotope compositions for the Sidi Driss and Douahria deposits (Decrée *et al.,* 2014). At a larger scale, the metal deposits in the Tellian/Nappe Zone formed at the turning point between late collisional events (Late Tortonian) and extensional regime (Early Messinian). Most of the deposits and showings are located close to the NE-SW Ghardimaou-Cap Serrat sinistral shear zone and related to transtensional reactivation of these structures and others inherited from the Variscan orogeny (and also possibly from the Pan-African orogeny; Piqué *et al.*, 2002), during the last phase of the Alpine orogeny (Upper Miocene; Jemmali *et al.*, 2013).

Re-evaluation of the possible classification of the Nefza Pb-Zn deposits as SedEx-type and MVT deposits

According to Decrée *et al.* (2008a, 2016), several characteristics of the Sidi Driss and Douahria deposits may favour their assignment to the SHMS-SedEx type rather than to the neighbouring MVT deposits, which form a large province in Tunisia. First, the stratabound texture of their ore with 'soft'-style sedimentary structures suggests synsedimentary formation. Then, the involvement of hot fluids is inferred, considering the homogenization temperature of the late calcite infillings that are between 160 and 190°C (in the NaCl–H$_2$O system, with a corresponding salinity of 11.7 to 18.3 wt.% NaCl equivalent). This fluid would be a late representative of the hot brines/fluids involved in the genesis of these deposits. Both stratabound/stratiform character with high temperature are also key attributes of SedEx deposits (e.g., Leach *et al.*, 2005; Wilkinson, 2014). Another feature of the Sidi Driss deposits is the Fe–Mn enrichment of early diagenetic carbonates, which emphasizes the inception of hydrothermal circulation at an early stage. The area of this Fe-Mn aureole, which is larger than the extent of base-metal enrichment, has been observed in Proterozoic Australian SedEx deposits (Large & McGoldrick, 1998). The same applies to the early deposition of barite at Sidi Driss (and its role as a sulphur source), which is also highlighted in several SedEx deposits (Kelley *et al.*, 2004; Piatak, 2004). However, it is worth mentioning major differences between the characteristics of these deposits, as the very low metal tonnage observed in the Tunisian deposits compared to SedEx deposits *sensu stricto*. The limiting factor for this low tonnage is likely the availability of base-metals, owing to the abundance of sulphates left in the system after sulphide deposition (Decrée *et al.*, 2008a). Other contrasting characteristics are related to the chemistry of sphalerite. Although an overlap of the Fe, Cd, Ge, Mn, Sb and Co contents can be considered for sphalerite from the Nefza and the SedEx type, major discrepancies are noted for Pb, Tl and Ni that are higher in the Nefza deposits, and Cu and In contents that are higher in the SedEx type (Fig. 3). One can also note that the S isotope composition differs in both deposit types. It is heavier – with a narrower range of composition (-5 to 15 per mil; Leach *et al.*, 2005) - for sphalerite from the SedEx deposits compared to sphalerite from Sidi Driss and Nefza (Fig. 4). The ultimate source of sulphur is marine sulphate and both BSR and TSR are involved in SedEx deposits, as is the case for the Sidi Driss and Douahria deposits. The isotopic fractionation trend towards heavier S, that is common in

the late stage of the paragenesis, could reflect closed conditions or the dominance of hydrothermal sulphur (Leach *et al.*, 2005).

In contrast, the trace element contents of sphalerite from the Nefza deposits largely overlap with those of MVT deposits, except for Ni (higher for the Nefza deposits) (Fig. 3). However, their S isotope composition differs significantly, with δ^{34}S being heavier for sphalerite and galena from the MVT deposits (Fig. 4). Such heavy sulphur was likely produced at depth by TSR from Triassic sulphates (e.g., Sheppard & Charef, 1990; Charef & Sheppard, 1991; Orgeval, 1994; Bechtel *et al.*, 1996). The range of δ^{34}S for sulphides observed for the Tunisian MVT deposits would be due to the mixing between this TSR-related sulphur and a lighter sulphur involving BSR (e.g., Sheppard *et al.*, 1996; Jemmali *et al.*, 2013). Although some common characteristics can be noted, the proposed genetic models for the Nefza mineralization and Tunisian MVT deposits are barely compatible. Most of the MVT deposits of the Dome zone are epigenetic deposits emplaced in Triassic and Middle-Upper Cretaceous carbonate rocks and breccias (e.g., Orgeval, 1994; Sheppard *et al.*, 1996; Jemmali *et al.,* 2013 and references therein), resulting from large-scale gravity-driven hydrothermal fluid circulation in connection with the late Alpine convergence during the Serravallian–Tortonian (Kyle & Posey, 1991; Perthuisot & Rouvier, 1996), whereas Sidi Driss and Douahria are syndiagenetic deposits formed through small-scale thermally-driven convection cells in a Messinian extensional context.

Concluding note: assignment of the Sidi Driss and Douahria Pb-Zn deposits as Irish-type deposits

The Sidi Driss and Douahria deposits present some features that relate them to SedEx type deposits and to MVT deposits for other features. Therefore, they can be considered as hybrid deposits between the SedEx and MVT, as are the Pb-Zn deposits hosted in carbonates of the Irish orefield (e.g., Piercey, 2013; Yesares *et al.*, 2019). Actually, the Nefza deposits could be considered to be Irish-type deposits. We will develop this concept by emphasizing the numerous similarities shared by both deposit types (Decrée *et al.*, 2008a as the main reference for the Nefza deposits).

(i) First, all these deposits (Nefza and Irish-type) are mostly stratabound and result from the replacement of carbonate rocks. Complex sulphide textures are observed in both deposit types; spherulitic and colloform texture of sphalerite is one of the most typical textures of the ore (e.g., Hitzman & Beaty, 1996; Wilkinson & Hitzman, 2014). In addition, the sphalerite from the Sidi Driss and Douahria deposits shares comparable Fe and Cd contents with the Irish-type (Navan deposits, Gagnevin *et al.*, 2014), with an overlap in As, Mn, Sb, Ga, and Cu concentration (note that the range of contents is particularly large for the Irish-type, with values varying from below detection limit to the values indicated by pentagons in Fig. 4).

(ii) Similarly, the δ^{34}S range of sphalerites from the Irish-type deposits largely overlaps the range of sphalerite from Sidi Driss and Douahria deposits (Fig. 4). This can be explained by the fact that BSR is the dominant sulphate reduction process in sphalerite formation in both deposit types (Fallick *et al.*, 2001;

Decrée *et al*., 2008a). This is also supported by the texture of sphalerite. Both in the Irish-type and in the Nefza deposits, a bimodal distribution of S isotopic composition is seen. It is linked to combined BSR (for the most negative $\delta^{34}S$) and TSR (for the most positive $\delta^{34}S$ values) (e.g., Anderson *et al*., 1998; Elliott *et al*., 2018). At Sidi Driss and Douahria, the alternating deposition of BSR and TSR-related sulphides is likely due to the mixing of shallow-basinal (with hypersaline/evaporated) Messinian seawater and deeper – hot – fluids. In the same way, the formation of the Irish-type deposits is related to the presence of two fluids: a brine resulting from seawater evaporation and a high temperature fluid that interacted with the basement (e.g., LeHuray *et al*., 1987; Everett *et al*., 1999; Banks *et al*., 2002; Wilkinson, 2010; Wilkinson & Hitzman, 2014).

(iii) In the Nefza district, the metal deposits are mostly located along varying structures created or reactivated under transtensional regime during the Early Messinian. The Irish-type mineral deposits are likewise controlled by inherited normal faults in a transtentional environment (Everett *et al*.,1999; Wilkinson & Hitzman, 2014), which acted as the main conduits for the metal-rich fluids (e.g., Ashton *et al*., 2003; Carboni *et al.,* 2003; McCusker & Reed, 2013; Torremans *et al*., 2018; Kyne *et al*., 2019).

(iv) The heat generated by alkaline magmatism in an extensional regime locally constitutes a driver for hydrothermal fluids for some of the Irish-type deposits (Davidheiser-Kroll *et al*., 2014; Wilkinson & Hitzman, 2014). In that context, the breccias associated with intrusive rocks (as in the Stonepark Prospect) facilitate the introduction of metal-rich fluids in the system (McCusker & Reed, 2013; Elliott *et al*., 2018). By analogy, in the Nefza district, Messinian mafic magmatism would trigger/favour a thermally driven fluid circulation (Decrée *et al*., 2008a). However, at a shallower level, the fluids were likely drained along major structural discontinuities (such as thrust sheet boundaries and magmatic contacts) that constitute the transport route metals for the mineralizing system (Decrée *et al*., 2008a).

(v) Another common characteristic of the Nefza Pb-Zn deposits and deposits in the Irish orefield is the enrichment in Mn and Ba, which is likely related to hydrothermal fluids (e.g., Hitzman & Beaty, 1996; Wilkinson *et al*., 2005, 2009, 2011). Its most visible expression is the Mn halo at the fringe of the orebody resulting from metal remobilization in the system (e.g., Wilkinson *et al*., 2011), as the manganiferous zone of the Tamra basin that partly overlies the Sidi Driss basin (Decrée *et al.,* 2010; Garnit *et al*., 2020).

Acknowledgments

References

Abidi, R., Slim-Shimi, N., Marignac, C., Somarin, A. K., Renac, C., Deloule, E., Hatira, N., & Gasquet, D., (2022) The microbial controls on the deposition of Pb-Zn minerals in carbonate-hosted Tunisian ore deposits. *Resource Geology,* v. 72(1), e12287.

Albidon Limited, (2004) Exploration Report. http://www.albidon.com/documents/Nefza2. pdf.

Anderson, I.K., Ashton, J.H., Boyce, A.J., Fallick, A.E., & Russell, M.J., (1998) Ore depositional processes in the Navan Zn+Pb deposit Ireland. *Economic Geology*, v. 93, 535–563.

Ashton, J.H., Holdstock, M.P., Geraghty, J.F., O'Keeffe, W.G., Martinez, N., Peace, W., & Philcox, M.E., (2003) The Navan orebody—discovery and geology of the South West Extension. In: Kelly, J.G., et al. (eds) Europe's Major Base Metal Deposits. Irish Association for Economic Geology, Dublin, 405– 436.

Badgasarian, G.P., Bajanik, S., & Vass, D., (1972) Age radiométrique du volcanisme néogène du Nord de la Tunisie. *Notes du Service Géologique de Tunisie*, v. 40, 79–85.

Baele, J.M., Bouzahzah, H., Papier, S., Decrée, S., Verheyden, S., Burlet, Ch., Pirard, E., Franceschi, G., & Dejonghe, L., (2021) Trace-element imaging at macroscopic scale in a Belgian sphaleritegalena ore using Laser-Induced Breakdown Spectroscopy (LIBS), *Geologica Belgica*, v. 24(3-4), 125-136.

Banks, D. A., Boyce, A. J., & Samson, I. M., (2002) Constraints on the origins of fluids forming Irish Zn-Pb-Ba deposits: Evidence from the composition of fluid inclusions. *Economic Geology*, v. 97(3), 471-480.

Barré, G., Truche, L., Bazarkina, E., Michels, R., & Dubessy, J., (2017) First evidence of the trisulfur radical ion S^{3-} and other sulfur polymers in natural fluid inclusions. *Chemical Geology*, v. 462, 1-14.

Barrett, T. J., & Anderson, G. M., (1988) The solubility of sphalerite and galena in 1–5 m NaCl solutions to 300 C. *Geochimica et Cosmochimica Acta*, v. 52(4), 813-820.

Batik, P., (1980) Carte géologique de la Tunisie; feuille n°11: Hédil. Service Géologique, Office National des Mines (1 sheet).

Belguith, Y., Geoffroy, L., Rigane, A., Gourmelen, C., & Ben Dhia, H., 2011. Neogene extensional deformation and related stress regimes in central Tunisia. *Tectonophysics*, v. 509, 198–207

Bechtel, A., Shieh, Y.-N., Pervaz, M., & Püttmann, W., (1996) Biodegradation of hydrocarbons and biogeochemical sulfur cycling in the salt dome environment: inferences from sulfur isotope and organic geochemical investigations of the Bahloul Formation at the Bou Grine Zn/Pb ore deposit, Tunisia. *Geochimica et Cosmochimica Acta*, v. 60, 2833–2855.

Bellon, H., (1976) Séries magmatiques néogènes et quaternaires du pourtour de la Méditerranée occidentale, comparées dans leur cadre géochronologique; implications géodynamiques. Unpublished Ph.D. Thesis. Paris South University, 367 pp.

Benaouali-Mebarek, N., Frizon de Lamotte, D., Roca, E., Bracene, R., Faure, J.-L., Sassi, W., & Roure, F., (2006) Post-Cretaceous kinematics of the Atlas and Tell systems in central Algeria: early foreland folding and subduction-related deformation. *Comptes Rendus Géosciences*, v. 338, 115–125.

Bodnar, R.J., (2003) Introduction to aqueous-electrolyte fluid inclusions. In: Samson, I., et al. (eds) Fluid inclusions: analysis and Interpretation. *Mineralogical Association of Canada Short Course Notes,* v. 32, 81–100.

Booth-Rea, G., Gaidi, S., Melki, F., Marzougui, W., Azañón, J. M., Zargouni, F., Galvé, J.P., & Pérez-Peña, J. V., (2018) Late Miocene extensional collapse of northern Tunisia. *Tectonics,* v. 37(6), 1626-1647.

Bouaziz, S., Barrier, E., Soussi, M., Turki, M.M., & Zouari, H., (2002) Tectonic evolution of the northern African margin in Tunisia from paleostress data and sedimentary record. *Tectonophysic*s, v. 357, 227–253.

Carboni, V., Walsh, J.J., Stewart, D.R.A., & Güven, J.F., (2003) Timing and geometry of normal faults and associated structures at the Lisheen Zn/Pb deposit, Ireland—Investigating their role in the transport and the trapping of metals. In: Eliopoulos, D., *et al.* (eds) Mineral Exploration and Sustainable Development. Millpress, Rotterdam, 665– 668.

Charef, A., & Sheppard, S.M.F., (1991) The diapir related Bou Grine Pb–Zn deposit (Tunisia): evidence for role of hot sedimentary basin brines. In: Pagel, M. & Leroy, J. (eds) Source, Transport and Deposition of Metals. Balkema, Rotterdam, 269–272.

Claypool, G., Holser, W., Kaplan, I., Sakai, H., & Zak, I., (1980) The age curves of sulfur and oxygen isotopes in marine sulfate and their mutual interpretation. *Chemical Geology*, v. 28, 199–260.

Davidheiser-Kroll, B., Stuart, F. M., & Boyce, A. J., (2014) Mantle heat drives hydrothermal fluids responsible for carbonate-hosted base metal deposits: Evidence from 3He/4He of ore fluids in the Irish Pb-Zn ore district. *Mineralium Deposita*, v. 49(5), 547-553.

Decrée, S., (2008) Caractérisation géochimique et isotopique dans un système d'altération complexe, du protolithe magmatique à la minéralisation fer plomb-zinc: le cas de la mine de Tamra (N. Tunisie). Unpublished Ph.D. thesis, Brussels University (ULB), 239 pp.

Decrée, S., Marignac, C., De Putter, Th., Deloule, E., Liégeois, J.P., & Demaiffe, D., (2008a) Pb–Zn mineralization in a Miocene regional extensional context: The case of the Sidi Driss and the Douahria ore deposits (Nefza mining district, northern Tunisia). *Ore Geology Reviews*, v. 34, 285–303.

Decrée, S., De Putter, Th., Yans, J., Recourt, Ph., Jamoussi, F., Bruyère, D., & Dupuis, Ch., (2008b) Iron mineralization in Pliocene sediments of the Tamra iron mine (Nefza mining district, Tunisia) - Mixed influence of pedogenesis and hydrothermal alteration. *Ore Geology Reviews*, v. 33, 397–410.

Decrée, S., Ruffet, G., De Putter, Th., Baele, J.M., Recourt, Ph., & Yans, J., (2010) Mn oxides as efficient traps for metal pollutants in a Fe–Pb–Zn mine environment (Tamra iron mine, Nefza mining district, Tunisia). *Journal of African Earth Sciences*, v. 57, 249–261.

Decrée, S., Baele, J.-M., De Putter, Th., Yans, J., Clauer, N., Dermech, M., Aloui, K., & Marignac, Ch., (2013) The Oued Belif hematite-rich breccia (Nefza Mining District, NWTunisia): a potential candidate for a Miocene small-scale iron oxide copper gold (IOCG) deposit in Northern Tunisia. *Economic Geology*, v. 108, 1425–1457.

Decrée, S., Marignac, C., Liégeois, J.P., Yans, J., Abdallah, R.B., & Demaiffe, D., (2014) Miocene magmatic evolution in the Nefza district (northern Tunisia) and its relationship with the genesis of polymetallic mineralizations. *Lithos,* v. 192, 240–258

Decrée, S., Marignac, C., Abidi, R., Jemmali, N., Deloule, E., & Souissi, F., (2016) Tectonomagmatic context of SedEx Pb-Zn and polymetallic ore deposits of the Nappe Zone northern Tunisia, and comparisons with MVT deposits in the region. In: Bouabdellah, M. & Slack, J. (eds) Mineral Deposits of North Africa. SGA special publication, Springer, 497-525.

Dekoninck, A., Moussi, B., Vennemann, T., Fakher, J., Mattielli, N., Decrée, S., Chaftar, H.R., Hatira, N., & Yans, J., (2018) Mixed hydrothermal and meteoric fluids evidenced by unusual H- and O-isotope compositions of kaolinite-halloysite in the Fe(-Mn) Tamra deposit (Nefza district, NW Tunisia). *Applied Clay Science*, v. 163. 10.1016/j.clay.2018.07.007

Dermech, M., (1990) Le complexe de l'Oued Bélif - Sidi Driss (Tunisie septentrionale). Hydrothermalisme et métallogénie. Unpublished PhD thesis. Paris VI University, 336 pp.

Elliott, H. A., Gernon, T. M., Roberts, S., Boyce, A. J., & Hewson, C., (2019) Diatremes act as fluid conduits for Zn-Pb mineralization in the SW Irish ore field. *Economic Geology*, v. 114(1), 117-125.

Everett, C. E., Wilkinson, J. J., & Rye, D. M., (1999) Fracture-controlled fluid flow in the lower Palaeozoic basement rocks of Ireland: Implications for the genesis of Irish-type Zn-Pb deposits. Geological Society of London, Special Publications, 155(1), 247-276.

Fallick, A.E., Ashton, J.H., Boyce, A.J., Ellam, R.M., & Russell, M.J., (2001) Bacteria were responsible for the magnitude of the world-class hydrothermal base metal sulfide orebody at Navan, Ireland. *Economic Geology*, v. 96, 885–890.

Faul, H., & Foland, K., (1980) L'âge des rhyodacites de Nefza-Sedjenane. Notes du Service Géologique de Tunisie n°46. *Travaux de Géologie Tunisienne,* v. 14, 47–49.

Filoche, C., & Flinois, J.S., (2007) Interférence de la réduction bactérienne des sulfates (BSR) et de la thermoréduction chimique (TSR) dans le cas d'une minéralisation sédimentaire de Zn–Pb (Sidi Driss, Tunisie): test par l'analyse isotopique du soufre par microsonde ionique. Unpublished Bachelor's thesis. Institut Polytechnique de Lorraine-Nancy, 31 pp.

Flecker, R., De Villiers, S., & Ellam, R. M., (2002) Modelling the effect of evaporation on the salinity–87Sr/86Sr relationship in modern and ancient marginal-marine systems: the Mediterranean Messinian Salinity Crisis. *Earth and Planetary Science Letters,* v. 203(1), 221-233.

Gagnevin, D., Menuge, J. F., Kronz, A., Barrie, C., & Boyce, A. J., (2014) Minor elements in layered sphalerite as a record of fluid origin, mixing, and crystallization in the Navan Zn-Pb ore deposit, Ireland. *Economic Geology,* v. 109(6), 1513-1528.

Garnit, H., Kraemer, D., Bouhlel, S., Davoli, M., & Barca, D., (2020) Manganese ores in Tunisia: Genetic constraints from trace element geochemistry and mineralogy. *Ore Geology Reviews*, v. 120, 103451.

Gharbi, M., (1977) Etude des minéralisations mercurifères de l'accident Ghardimaou-Cap Serrat (Tunisie du Nord-Ouest). Unpublished MSc thesis. Ecole Nationale Supérieure de Géologie Appliquée et de Prospection Minière de Nancy, 131 pp.

Gottis, Ch., & Sainfeld, P., (1952) Les gîtes métallifères tunisiens: XIXème Congrès Géologique International. *Monographies régionales, 2e série, Tunisie,* 2, 104 pp.

Hitzman, M.W., & Beaty, D.W., (1996) The Irish Zn-Pb-(Ba) orefield: *Society of Economic Geologists, Special Publication,* 4, 112–143.

Hu, Y., Wei, C., Ye, L., Huang, Z., Danyushevsky, L., & Wang, H., (2021) LA-ICP-MS sphalerite and galena trace element chemistry and mineralization-style fingerprinting for carbonate-hosted Pb-Zn deposits: Perspective from early Devonian Huodehong deposit in Yunnan, South China. *Ore Geology Reviews,* v. 136, 104253.

Jaeger, J.-J., (1977) Les rongeurs du Miocène moyen et supérieur du Maghreb. *Palaeovertebrata,* v. 8(1), 1–166.

Jallouli, C., & Mickus, K., (2000) Regional gravity analysis of the crustal structure of Tunisia. *Jour of African Earth Sciences*, v. 30, 53–78.

Jallouli, C., Inoubli, M.H., & Alboui, Y., (1996) Le corps igné de Nefza (Tunisie septentrionale): caractéristiques géophysiques et discussion duMécanisme de samise en place. *Notes du Service Géologique de Tunisie,* 109–123.

Jallouli, C., Mickus, K., Turki, M.M., & Rihane, C., (2003) Gravity and aeromagnetic constraints on the extent of Cenozoic rocks within the Nefza–Tabarka region, northwestern Tunisia. *Journal of Volcanology and Geothermal Research*, v. 122, 51–68.

Jemmali, N., Souissi, F., Carranza, E.J.M., & Vennemann, T.W., (2013) Sulfur and lead isotopes of Guern Halfaya and Bou Grine deposits (Domes zone, northern Tunisia): implications for sources of metals and timing of mineralization. *Ore Geology Reviews*, v. 54:17–28

Jolivet, L., (2008) Géodynamique méditerranéenne. In: Jolivet, L., et al. (eds) Géodynamique méditerranéenne. *Société Géologique de France, Vuibert*, 5–47.

Kelley, K., Leach, D., Johnson, C., Clark, J., Fayek, L., Slack, J., Anderson, V., Ayuso, R., & Ridley, W., (2004) Textural, compositional, and sulfur isotope variations of sulfide minerals in the Red Dog Zn–Pb–Ag deposits, Brooks Range, Alaska: implications for ore formation. *Economic Geology*, v. 99, 1509–1532.

Khomsi, S., Soussi, M., Mahersi, C., Bedir, M., Fakhfakh-Ben Jemina, H., Riahi, S., & Bou Khalfa, K., (2009) New insights on the structural style of the subsurface of the Tell units in north-western Tunisia issued from seismic imaging: geodynamic implications. *Comptes Rendus Géosciences*, v. 341, 347–356

Kucha, H., Schroll, E., Raith, J. G., & Halas, S. (2010). Microbial sphalerite formation in carbonate-hosted Zn-Pb ores, Bleiberg, Austria: micro-to nanotextural and sulfur isotope evidence. *Economic Geology*, v. 105(5), 1005-1023.

Kyle, J. & Posey, H., (1991) Halokinesis, cap rock development, and salt dome mineral resources. In: Melvin, J. (ed) Evaporites, Petroleum and Mineral Resources. Elsevier, Amsterdam, 445–469.

Kyne, R., Torremans, K., Güven, J., Doyle, R., & Walsh, J., (2019) 3-D modeling of the Lisheen and Silvermines deposits, County Tipperary, Ireland: Insights into structural controls on the formation of Irish Zn-Pb deposits. *Economic Geology*, v. 114(1), 93-116.

Large, R., & McGoldrick, P., (1998) Lithogeochemical halos and geochemical vectors to stratiform sediment hosted Zn–Pb–Ag deposits. Part 1: Lady Loretta deposit, Queensland. *Journal of Geochemical Exploration*, v. 63, 37–56.

Laridhi Ouazaa, N., (1996) Etude minéralogique et géologique des épisodes magmatiques mésozoïques et miocènes de la Tunisie. Unpublished PhD thesis. Université de Tunis II, 466 pp.

Leach, D.L., Sangster, D.F., Kelley, K.D., Large, R.R., Garven, G., Allen, C.R., Gutzmer, J. & Walters, S., (2005) Sediment-hosted lead–zinc deposits: a global perspective. *In*: Hedenquist, J.W*., et al.* (eds) Economic Geology 100th Ann Vol 1905–2005. Soc Economic Geologists, Littleton, Colorado, USA, 561–607.

LeHuray, A. P., Caulfield, J. B. D., Rye, D. M., & Dixon, P. R., (1987) Basement controls on sediment-hosted Zn-Pb deposits; a Pb isotope study of Carboniferous mineralization in central Ireland. *Economic Geology*, v. 82(7), 1695-1709.

Machel, H., (2001) Bacterial and thermochemical sulfate reduction in diagenetic settings — old and new insights. *Sedimentary Geology*, 140, 143–175.

Mauduit, F., (1978) Le volcanisme néogène de la Tunisie continentale. Unpublished Ph.D. thesis. Paris South University, 157 pp.

Maury, R.C., Fourcade, S., Coulon, C., El Azzouzi, M., Bellon, H., Coutelle, A., Ouabadi, A., Semroud, B., Megartsi, M., Cotten, J., Belanteur, O., Louni-Hacini, A., Piqué, A., Capdevila, R., Hernandez, J., & Réhault, J.-P., (2000) Post-collisional Neogene magmatism of the Mediterranean Maghreb margin: a consequence of slab breakoff. *Comptes Rendus de l'Académie des Sciences*, v. 331, 159–173.

McCusker, J., & Reed, C., (2013) The role of intrusions in the formation of Irish-type mineralisation. *Mineralium Deposita*, v. 48(6), 687-695.

Melki, F., Zargouni, F., Chelbi, M.B., Bédir, M. & Zouaghi, T., (2012) Role of the NE-SW Hercynian master fault systems and associated lineaments on the structuring and evolution of the Mesozoic and Cenozoic basins of the Alpine margin, northern Tunisia. In: Shark, E. (ed) Tectonics-Recent Advances. doi:10.5772/50145

Mickus, K., & Jallouli, C., (1999) Crustal structure beneath the Tell and Atlas Mountains (Algeria and Tunisia) through the analysis of gravity data. *Tectonophysics*, v. 314, 373–385.

Negra, L., (1987) Pétrologie, minéralogie et géochimie des minéralisations et des roches encaissantes des bassins associés aux structures tectoniques et magmatiques de l'Oued Bélif et du Jebel Haddada (Nord des Nefza, Tunisie septentrionale). Unpublished Ph.D. thesis. Paris-Sud University, 223 pp.

Orgeval, J.J., (1994) Peridiapiric metal concentration: example of the Bou Grine deposit (Tunisian Atlas). In: Fontbote, L. & Boni,M. (eds) Sediment-hosted Zn–Pb ores. SGA Special Publication. Springer-Verlag, Berlin-Heidelberg, 10, 354–389.

Ould Bagga, M.A., Abdeljaouad, D., & Mercier, E., (2006) La « zone des nappes » de Tunisie: une marge méso-cénozoïque en blocs basculés modérément inversée (région de Taberka/Jendouba; Tunisie nord-occidentale). *Bulletin de la Société Géologique de France,* v. 177, 145–154.

Paytan, A., Kastner, M., Campbell, D., & Thielmens, M., (1998) Sulfur isotopic composition of Cenozoic seawater sulfate. *Science,* v. 282, 1459–1462.

Perthuisot, V., & Rouvier, H., (1996) Les dépôts Pb–Zn associés aux évaporites du Trias des diapirs du Maghreb oriental (Tunisie). 16ème Réunion des Sciences de la Terre, Orléans. Société Géologique de France, Paris, p. 158.

Piatak, N., (2004) Environmental significance of cadmium and other trace element concentrations in sphalerite from mineral deposits. *Geological Society of America*, Abstracts with Program, 36(5), p. 27.

Piercey, S., (2013) Economic Geology Blog. Irish-type deposits. Accessed on December 1, 2022. https://stevepiercey.wordpress.com/category/irish-type-deposits

Piqué, A., Ait Brahim, L., El Azzouzi, M.H., Maury, R., Bellon, H., Semroud, B., & Laville, E., (1998) Le poinçon maghrébin: contraintes structurales et géochimiques. *Comptes Rendus de l'Académie des Sciences*, v. 326, 575–581.

Piqué, A., Tricart, P., Guiraud, R., Laville, E., Bouaziz, S., Amrhar, M., & Ait Ouali, R., (2002) The Mesozoic–Cenozoic Atlas belt (North Africa): an overview. *Geodinamica Acta*, v. 15, 185–208.

Roman, F., & Solignac, M., (1934) Découverte d'un gisement de Mammifères pontiens à Douaria (Tunisie septentrionale). *Comptes-Rendus de l'Académie des Sciences*, 199, 1649–1659.

Rouvier, H., (1977) Géologie de l'extrême Nord Tunisien: tectonique et paléogéographie superposées à l'extrémité orientale de la chaîne Nord-Maghrebine. Unpublished Ph.D. thesis. Pierre et Marie Curie University, 215 pp.

Rouvier, H., (1987) Carte géologique de la Tunisie; feuille n°10: Nefza. Service Géologique, Office National des Mines.

Rouvier, H., (1994) Notice explicative de la carte géologique de la Tunisie au 1/50000e -Nefza, feuille 10. Office National des Mines, Direction de la Géologie. 48 pp.

Sainfeld, P., (1952) Les gîtes plombo-zincifères de Tunisie. *Annales des Mines et de la Géologie,* v. 9, 285.

Sanz-Rubio, E., Sánchez-Moral, S., Cañaveras, J.C., Calvo, J.P., & Rouchy, J.M., (2001) Calcitization of Mg–Ca carbonate and Ca sulphate deposits in a continental Tertiary Basin (Calatayud Basin, NE Spain). *Sedimentary Geology*, v. 140, 123–142.

Schroll, E., (1996) The Triassic carbonate-hosted Pb–Zn mineralization in the Alps (Europe): the genetic position of Bleiberg type deposit. In: Sangster, D.F. (ed) Carbonate-hosted lead–zinc deposits. *SEG Special Publication*, 4, 182–194.

Seward, T.M. & Barnes, H.L., (1997) Metal transport by hydrothermal ore fluids, In: Barnes, H.L. (ed) Geochemistry of Hydrothermal Ore Deposits, 3rd edition. Wiley, New York, 435–486.

Sheppard, S.M.F. & Charef, A., (1990) Isotopic studies (H,C,O, S, Pb) on carbonate shale hosted Pb–Zn deposits. In: Pélissonnier,H. & Sureau, J.F. (eds) Mobilité et concentration des métaux de base dans

les couvertures sédimentaires. Manifestations, mécanismes, prospection. *Documents du BRGM*, v. 183, 37–49.

Sheppard, S., Charef, A. & Boulhel, S., (1996) Diapirs and Pb–Zn mineralization: a general model based on Tunisian (N. Africa) and Gulf Coast (U.S.A.) deposits. In: Sangster, D. (ed) Carbonate-hosted lead–zinc deposits: *Society of Economic Geologists,* Special Publication, 4, 230–243.

Torremans, K., Kyne, R., Doyle, R., Güven, J. F., & Walsh, J. J., (2018) Controls on metal distributions at the Lisheen and Silvermines deposits: insights into fluid flow pathways in Irish-type Zn-Pb deposits. *Economic Geology*, v. 113(7), 1455-1477.

Warr, L. N., (2021) IMA–CNMNC approved mineral symbols. *Mineralogical Magazine*, v. 85(3), 291-320.

Wilkinson, J. J., (2014) Sediment-hosted zinc–lead Mineralization: Processes and perspectives. Treatise on Geochemistry, 13, 219–249. https:// doi.org/10.1016/B978-0-08-095975-7.01109-8

Wilkinson, J. J., Hitzman, M. W., (2015) The Irish Zn-Pb orefield: the view from 2014. In: Archibald, S. M., & Piercey, S Current Perspectives on Zinc Deposits. *Irish Association for Economic Geology, Dublin,* 59-72.

Wilkinson, J. J., Eyre, S. L., & Boyce, A. J., (2005) Ore-forming processes in Irish-type carbonate-hosted Zn-Pb deposits: Evidence from mineralogy, chemistry, and isotopic composition of sulfides at the Lisheen mine. *Economic Geology,* v. 100(1), 63-86.

Wilkinson, J.J., Stoffell, B., Wilkinson, C.C., Jeffries, T.E., & Appold, M.S., (2009) Anomalously metal-rich fluids form hydrothermal ore deposits. *Science,* v. 323, 764–767.

Wilkinson, J. J., Crowther, H. L., & Coles, B. J., (2011) Chemical mass transfer during hydrothermal alteration of carbonates: Controls of seafloor subsidence, sedimentation and Zn–Pb mineralization in the Irish Carboniferous. *Chemical Geology*, v. 289(1-2), 55-75.

Yans, J., Verhaert, M., Gautheron, C., Antoine, P.O., Moussi, B., Dekoninck, A., Decrée, S., Chaftar, R., Hatira, N., Dupuis, C., Pinna-Jamme, R., & Jamoussi, F., (2021) (U-Th)/He Dating of Supergene Iron (Oxyhydr- Oxides of the Nefza-Sejnane District (Tunisia): New Insights into Mineralization and Mammalian Biostratigraphy. *Minerals,* v. 11, 260. https://doi.org/10.3390/min11030260

Yesares, L., Drummond, D. A., Hollis, S. P., Doran, A. L., Menuge, J. F., Boyce, A. J., & Ashton, J. H., (2019) Coupling mineralogy, textures, stable and radiogenic isotopes in identifying ore-forming processes in Irish-type carbonate-hosted Zn–Pb deposits. *Minerals*, v. 9(6), 335.

Analytical Methods

The petrographic description is based on optical microscopy and scanning electron microscopy (SEM) using a Quanta 20 ESEM (FEI), with energy-dispersive spectroscopy (Apollo 10 silicon drift EDS detector; EDAX) at the Royal Belgian Institute of Natural Sciences.

Elemental imaging at macroscopic scale was performed using a LIBS (Laser-Induced Breakdown Spectroscopy) system developed at Geology and Applied Geology Dept., university of Mons, Belgium. Methodological detail for the application of LIBS to a sulphide ore sample is given in Baele *et al.* (2021). In short, high-energy laser pulses were fired at 20 Hz repetition rate and focused on the sample surface. The sample was continuously moving in a raster scan mode at such a speed that the distance (lateral resolution) between the laser shots was 100 μm. The optical spectrum of the plasma induced by laser-matter interaction at each spot on the sample surface was acquired with a delay of 1 μs after the laser shot. Then, the dataset, which consists in a hyperspectral datacube (two spatial and one spectral dimension) was processed to extract the intensities of atomic emission lines of interest (Pb, Zn, etc.) to produce elemental images with 100 μm pixel size.

The LA-ICP-MS was performed at the KU Leuven earth and environmental sciences department using a Teledyne Cetac 193nm laser ablation system with a HellEx II cell, coupled to an Agilent 8900 triple quad ICP-MS. 50μm spots were analysed at a rate of 2.7J/cm² for 1 minute at a repetition rate of 10 Hz, 15s of blank were measured before each sample. The following isotopes were measured on the ICP-MS ^{34}S, ^{55}Mn, ^{56}Fe, ^{59}Co, ^{60}Ni, ^{63}Cu, ^{64}Zn, ^{66}Zn, ^{71}Ga, ^{72}Ge, ^{75}As, ^{77}Se, ^{78}Se, ^{95}Mo, ^{111}Cd, ^{115}In, ^{121}Sb, ^{125}Te, ^{197}Au, ^{205}Tl, ^{208}Pb for 5-50ms depending on their concentration. NIST 610, 612 and MASS-1 were used for external calibration for the major element of the sulphide (Cu, Sn, …) was used as well as internal standards. Background correction and quantification was done using HDIP.

The fluid inclusion study was performed at the Department of Earth and Environmental Sciences of the Katholieke Universiteit in Leuven (Laboratory of P. Muchez, using a Linkam THMSG 600 stage coupled to an Olympus BX60 microscope; see details in Decrée, 2008).

Measurements of sulphur isotope compositions were performed in-situ with an ion microprobe at Centre de Recherches Pétrographiques et Géochimiques–CRPG in Nancy (see Decrée *et al*., 2008a, for details about the methods).

Supplemental Material -1

Summary of the statistical data from the Nefza district measured on the dataset comprising apatite analyses (LA-ICPMS analyses and bulk analyses of concentrates/separates)

	Mn	Co	Cu	Ga	As	Sb	Pb	Cd	Fe	Ni	Ge	Mo	In	Tl
Perc 5	0.24	0.29	1.8	0.66	8.1	0.20	1089	790	555	0.23	0.35	0.20	0.02	72
Perc 25	1.6	0.63	6.7	1.8	37	0.78	1620	2173	1276	6.6	0.54	0.48	0.05	114
Mediane	17	7.5	19	2.6	127	3.2	2016	2704	3048	14	15	0.97	0.18	353
Perc 75	77	9.4	47	24	701	4.5	3766	4355	9664	22	24	4.0	2.7	1537
Perc 95	151	20	93	46	1683	45	6307	4982	14601	41	681	7.4	13	7161

Supplemental Material – 2

Representative in-situ analyses (EPMA and LA-ICPMS or bulk analyses of separates/concentrates) of apatite from European phosphate deposits.

Median Values (ppm)	Sample	Mn	Fe	Co	Ni	Cu	Zn	Ga	Ge	As	Cd	In	Sb	Tl	Pb
Fe sulphides	SD2a_Py1	0.43		<d.l.	<d.l.	<d.l.	16.77	<d.l.	0.79	197.43	<d.l.	<d.l.	0.26	1174.66	5022.64
	SD2a_Py2	0.45		<d.l.	<d.l.	0.09	20.87	<d.l.	0.78	137.38	<d.l.	<d.l.	0.19	1156.18	5427.76
	SD2a_Py3	0.39		<d.l.	<d.l.	<d.l.	13.81	<d.l.	0.83	550.90	<d.l.	<d.l.	0.40	1511.56	6418.98
	PY5_Py1	123.06		<d.l.	<d.l.	<d.l.	16.51	0.02	0.31	158.76	<d.l.	<d.l.	0.07	609.42	3.81
	PY5_Py2	299.28		<d.l.	<d.l.	<d.l.	4.68	<d.l.	1.43	1073.27	<d.l.	<d.l.	0.09	2025.44	2.68
	SD2a_Ga1	0.04	11.19	<d.l.	<d.l.	<d.l.	7.80	<d.l.	0.15	782.72	3.89	<d.l.	682.93	25.84	
	SD2a_Ga2	0.02	14.16	0.02	<d.l.	<d.l.	2.12	<d.l.	0.10	542.42	6.93	<d.l.	676.81	15.50	
	SD2a_Ga3	0.03	21.13	<d.l.	0.27	<d.l.	14.19	<d.l.	0.22	1627.54	14.36	<d.l.	155.61	99.77	
	SD2a_Ga4	1.35	21.65	0.02	<d.l.	0.38	0.69	<d.l.	0.47	1218.46	<d.l.	<d.l.	6.73	2480.58	
	SD2a_Ga5	0.03	11.57	<d.l.	<d.l.	1.00	12.21	<d.l.	0.13	4140.72	34.18	<d.l.	29.29	346.79	
	SD2_Ga1	0.06	41.63	0.03	<d.l.	0.75	10.72	<d.l.	0.12	4471.73	17.57	<d.l.	9.19	316.33	
	SD2_Ga2	3.55	23.06	<d.l.	<d.l.	0.09	1.15	<d.l.	0.46	1589.57	<d.l.	<d.l.	0.77	2185.75	
Galena	DSU1_Ga1	0.06	15.67	<d.l.	<d.l.	<d.l.	3.86	<d.l.	0.11	261.21	8.52	<d.l.	0.20	38.70	
	DSU1_Ga2	1.53	10.67	<d.l.	<d.l.	0.39		<d.l.	0.37	52.39	<d.l.	<d.l.	<d.l.	62.50	
	DSU2a_Ga1	0.07	30.37	0.03	<d.l.	<d.l.		<d.l.	0.11	149.10	49.27	<d.l.	<d.l.	28.09	
	DSU2a_Ga2	0.01	6.95	<d.l.	<d.l.	0.10	2.68	<d.l.	0.14	1561.28	25.61	<d.l.	<d.l.	51.61	
	DSU2b_Ga1	0.08	40.41	<d.l.	<d.l.	0.41	4.06	<d.l.	0.13	553.70	24.67	<d.l.	5.45	18.20	
	DSU6a_Ga2	0.45	11.05	<d.l.	<d.l.	<d.l.	0.75	<d.l.	0.35	1.66	<d.l.	<d.l.	<d.l.	668.82	
	DSU6a_Ga3	0.11	41.16	0.08	<d.l.	0.52	21.02	<d.l.	0.10	11.06	22.91	<d.l.	0.03	290.51	
	DSU6b_Ga1	0.09	59.61	0.03	<d.l.	<d.l.	16.00	<d.l.	0.11	26.56	36.74	<d.l.	0.20	30.30	
	SD2a_Sp1	0.78	15304.31	0.27	0.24	1.72		0.68	3.31	127.08	594.88	<d.l.	1.06	352.83	1235.55
	SD2a_Sp2	63.87	13897.30	2.37	8.72	135.43		51.94	15.06	670.69	2704.31	0.18	4.60	327.95	1109.57
	SD2a_Sp3	0.26	215.52	<d.l.	<d.l.	1.94		0.64	14.65	304.87	5083.58	<d.l.	3.69	145.74	2011.36
	SD2a_Sp4	161.15	4065.26	0.63	<d.l.	11.37		39.65	1009.29	1988.94	2323.73	4.62	37.69	8119.65	3641.39
	SD2a_Sp5	0.21	894.04	<d.l.	<d.l.	2.01		2.58	30.05	730.87	4881.18	0.06	3.22	368.46	2591.78
Sphalerite	SD2a_Sp6	140.57	10912.59	0.31	0.23	23.01		11.99	353.51	1376.22	2681.17	16.87	53.08	6201.74	7651.47
	DSU6a_Sp1	17.07	3048.16	8.73	18.44	47.99		2.26	0.31	8.70	3008.91	<d.l.	0.28	69.41	2003.46
	DSU6a_Sp2	90.10	1313.63	7.54	32.50	17.26		36.23	18.67	54.60	984.42	0.77	3.07	2598.75	2016.02
	DSU6a_Sp3	41.43	8414.71	25.91	45.88	50.28		4.57	0.54	19.29	2021.42	0.02	0.49	82.05	4962.03
	DSU6a_Sp4	10.30	1739.32	9.40	9.59	18.94		1.95	0.53	116.95	4863.37	0.03	4.39	475.86	3889.97
	DSU6b_Sp1	2.48	1238.12	12.08	18.28	45.89		1.72	0.38	7.45	3845.88	<d.l.	0.11	75.50	1067.95
Detection Limit (ppm)		0.02	5.53	0.03	0.24	0.08	1.18	0.01	0.04	0.32	0.07	0.01	0.03	0.01	5.83